PNAS
www.pnas.org

Supplementary Information for

Thickness Scaling of Ferroelectricity in $BiFeO_3$ by Tomographic Atomic Force Microscopy

James J. Steffes, Roger A. Ristau, Ramamoorthy Ramesh, Bryan D. Huey

Corresponding Author: Bryan D. Huey
Email: bryan.huey@uconn.edu

This PDF file includes:

Supplementary text
Figs. S1 to S10
References for SI reference citations

Other supplementary materials for this manuscript include the following:

None

www.pnas.org/cgi/doi/10.1073/pnas.1806074116

Supplementary Information Text

Materials and Methods

The KrF laser fluence during $BiFeO_3$ film growth was 1.1 J cm^{-2}. The $SrRuO_3$ layer in the $BiFeO_3$ heterostructure functions as a conductive electrode which provides an efficient current and grounding path for scanning probe electrical measurements. The structure of the $BiFeO_3$ film was confirmed using x-ray diffraction, and cross sectional TEM was used to verify thickness of the as-grown $BiFeO_3$ and $SrRuO_3$ films. High-resolution TEM, high-angle annular darkfield scanning TEM (HAADF-STEM), and energy dispersive x-ray spectroscopy (EDXS) were performed on a Thermo-Fisher Scientific FEI (Hillsboro, OR USA) Talos F200X microscope operating at an accelerating voltage of 200 kV and equipped with an Amptek (Bedford, MA USA) Super-X SDD EDXS detector.

Single-frequency and dual-frequency PFM was performed in contact imaging mode and ambient conditions at the second eigenmode of the tip-sample normal and torsional contact resonance, ~2.2 MHz and ~2.3 MHz, respectively. PFM imaging was acquired using an AC amplitude of 1.0 V and a variable DC voltage bias ranging from 0.6 to 3.0 V DC at a linear scan speed of ~200 μm s^{-1}. PFM switching sequences were performed at a cantilever downforce of ~1 microNewton. The long axis of the cantilever was aligned parallel to the $[1\bar{1}0]$ $BiFeO_3$ direction in all PFM experiments. Probe current is detected during tomographic AFM using an Oxford Instruments Asylum Research ORCA module with an amplifier gain of 10^9 and a sample bias of 4.0 V DC. All tomographic reconstruction, image processing and data analysis were performed using MATLAB software (Mathworks, Natick, MA USA).

Three-Dimensional Landau-Ginzburg-Devonshire Theory for tomographic AFM

For this derivation, the following conventions are used: the directional indices $_1$, $_2$, and $_3$ correspond to the [100], [010], and [001] crystal directions, respectively. The [001]/[001]$_{pc}$ direction corresponds to the growth direction and surface normal of the $BiFeO_3$ heterostructure studied. The thermodynamic theory of crystals states that the strain produced along the [001] direction in a non-centrosymmetric crystal class by the converse piezoelectric effect under the influence of an electric field applied along the [001] direction is equal to

$$x_{33} = d_{33}E_3, \tag{1}$$

where x_{33} is the [001]-oriented normal crystal strain, d_{33} is the converse piezoelectric coefficient in units m V^{-1}, and E_3 is the [001]-oriented electric field in units V m^{-1}. This expression describes both oscillating and static effects. If one was to consider only the oscillating component of the applied electric field, Eq. 1 could be rewritten as

$$x_{33}^{\omega} = d_{33}E_3^{\omega}, \tag{2}$$

where the superscript ω refers to the indicated quantity at an oscillation frequency, ω. The oscillating component of the piezoelectrically-induced strain is of importance for this work since oscillatory strains can be effectively measured by an atomic force microscope (AFM). In the AFM mode of piezoresponse force microscopy (PFM), an oscillating (AC) voltage is applied to a conductive probe in contact with a piezoelectric sample, and the resulting surface displacement (i.e. strain) produced by the converse piezoelectric effect is transduced by the AFM cantilever. Since piezoelectric displacements in thin film structures are often small (< 100 pm), lock-in amplification is often utilized to improve measurement quality. An alternate derivation of Eq. 2 can be written to describe the converse piezoelectric effect as induced and measured by during PFM imaging,

$$u_3^{\omega} = d_{33}V^{\omega} = d_{33}V_{AC}\cos(\omega t + \phi), \tag{3}$$

where u_3^{ω} is the [001]-oriented surface displacement measured at frequency ω, also called the *piezoresponse*, and V^{ω} is the oscillating voltage applied between the AFM probe and sample at frequency ω. Often, there is a phase offset between the displacement signal and driving voltage, which is accounted for in the $\cos(\omega t + \phi)$ term. To improve the signal-to-noise ratio during PFM, the driven frequency is chosen to be at either the first or second eigenmode of the tip-sample contact resonance, which provides amplification of the piezoelectric actuation.

Neglecting electrostrictive effects and at zero applied DC electric field, the elastic strain induced by the spontaneous polarization under an oscillating electric field in a monodomain, poled ferroelectric is

$$x_{33}^{\omega} = 2Q_{33}\epsilon_0\epsilon_{33}P_s(h)\cdot E_3^{\omega}(h), \tag{4}$$

where ε_0 is vacuum permittivity, Q_{33} and ε_{33} are [001]-oriented components of the electrostriction and dielectric permittivity tensors, respectively, h is the crystal thickness, $P_s(h)$ is the thickness-dependent spontaneous polarization, and $E_3^{\omega}(h)$ is the oscillating applied electric field which is by definition thickness dependent. Employing the definition of engineering strain, the [001]-oriented strain at frequency ω can be defined as

$$x_{33}^{\omega} = \frac{\Delta h_3^{\omega}}{h_3} = \frac{u_3^{\omega}}{h_3}. \tag{5}$$

Assuming that the piezoelectric displacement transduced by the cantilever in the [001]-direction is primarily influenced by the [001]-component of the spontaneous polarization, $P_3(h) = P_s(h)$, and using $E_3^{\omega} = V^3/h$, the crystal strain can be expressed as the [001]-oriented displacement by combining Eq. 4 and Eq. 5,

$$u_3^{\omega} = 2Q_{33}\epsilon_0\epsilon_{33}P_3(h)\cdot V^{\omega} \tag{6}$$

which is similar in form to Eq. 3, with the inclusion of an additional term describing the thickness-dependent spontaneous polarization. Employing the three-dimensional derivation of

equilibrium Landau-Ginzburg-Devonshire theory presented by Rault, et al(1) for $BiFeO_3$, the normalized [001]-component of the spontaneous polarization can be written as

$$\frac{P_3}{P_{3,\max}} = A\sqrt{B + \sqrt{1 - \frac{h_{\mathrm{cr}}}{h}}} \tag{7}$$

where A and B are temperature-dependent constants that subsume multiple coefficients from the Landau free energy expansion with respect to spontaneous polarization, and h_{cr} is the critical thickness for ferroelectricity in the crystal. Eq. 7 can finally be combined with Eq. 6 to arrive at a relation describing the piezoelectric surface displacement at frequency ω as a function of crystal thickness, h

$$\frac{u_3^{\omega}}{u_{3,\max}^{\omega}} = 2Q_{33}\epsilon_0\epsilon_{33}V^{\omega} \cdot A\sqrt{B + \sqrt{1 - \frac{h_{\mathrm{cr}}}{h}}}. \tag{8}$$

Under the assumption of constant electrostriction and dielectric permittivity within the $BiFeO_3$ thickness range measured, Eq. 8 provides a means for investigating the spontaneous polarization in a non-uniaxial ferroelectric (i.e. $BiFeO_3$) as a function of film thickness using PFM.

Supplementary Figures S1-S10

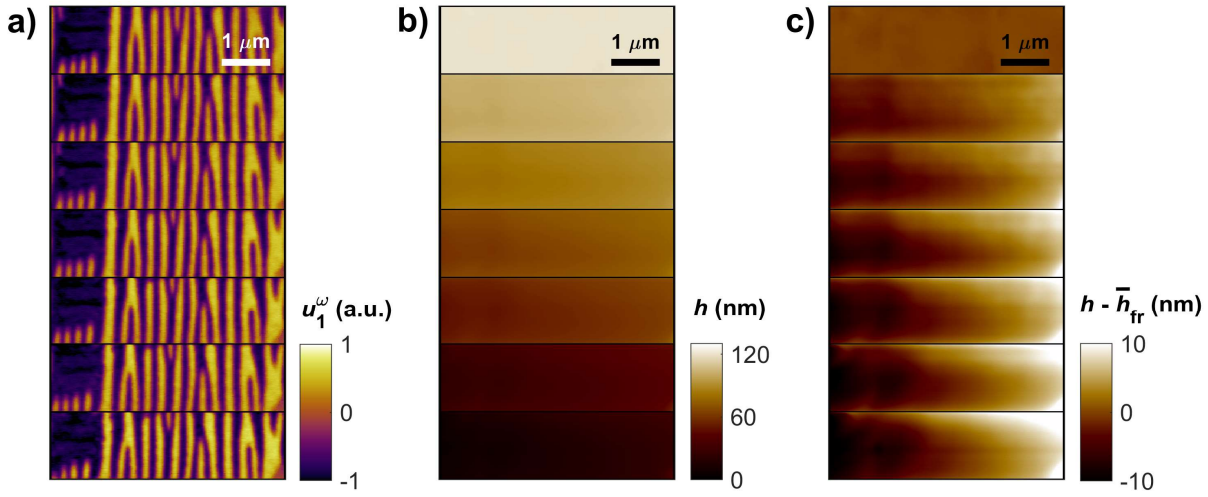

Fig. S1. Montage of consecutive tomographic AFM images (every ~20th frame) from which the tomogram of main paper Fig. 2*B* is constructed. a) In-plane piezoresponse contrast (u_1^ω) identifies alternating domains oriented along $[\bar{1}1\bar{1}]_{pc}$ and $[\bar{1}\bar{1}\bar{1}]_{pc}$. b) Simultaneously acquired topography (film thickness, *h*) showing near-complete removal of the $BiFeO_3$ film in the last (bottom) image frame. c) Identical topography data as panel *B* calculated as the differential between individual pixel values and the mean film thickness of the imaging frame, to assist in visualization of non-uniform local topography formed during tomographic processing.

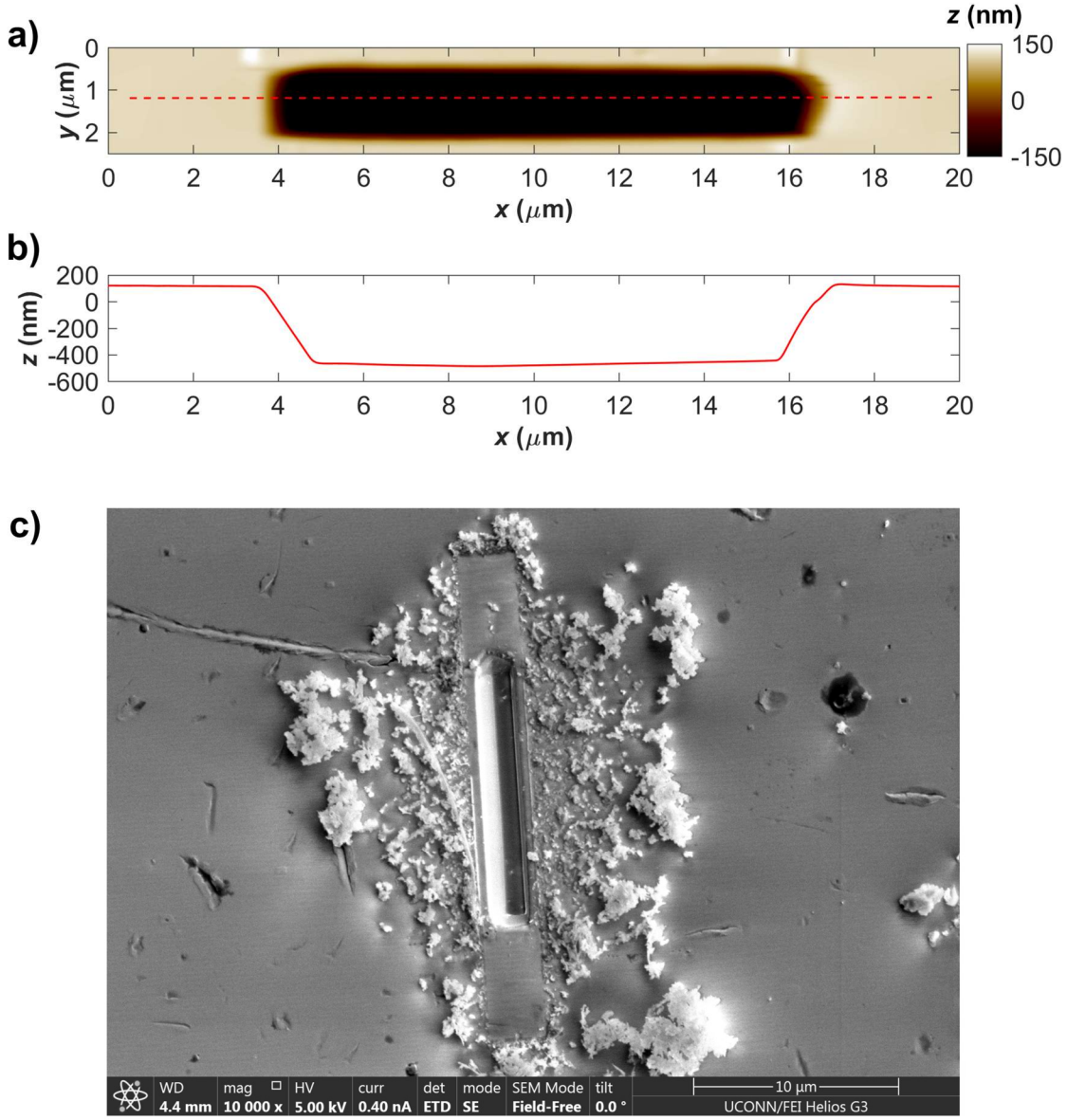

Fig. S2. Surface topography of h = 120 nm $BiFeO_3$ following tomographic AFM. a) spatial map of topography relative to the as-grown surface (z = 0 nm), b) line scan taken from the dashed red line in panel a). The subtractive nature of tomographic AFM is clearly evident in panels a) and b), wherein the areas where tomographic AFM were performed show a pronounced and well-defined region where the surface topography has been modified through $BiFeO_3$ film removal. As shown in panel b), the h = 120 nm $BiFeO_3$ film has been removed throughout the majority of the imaging field of view selected during tomographic AFM (x-y = 10 μm by 1.25 μm). c) Scanning electron microscope image of the post-tomography region of $BiFeO_3$ shown in panel a) (rotated by 90°). The $BiFeO_3$ that has been subtractively removed can be seen redeposited on the surface of the surrounding $BiFeO_3$.

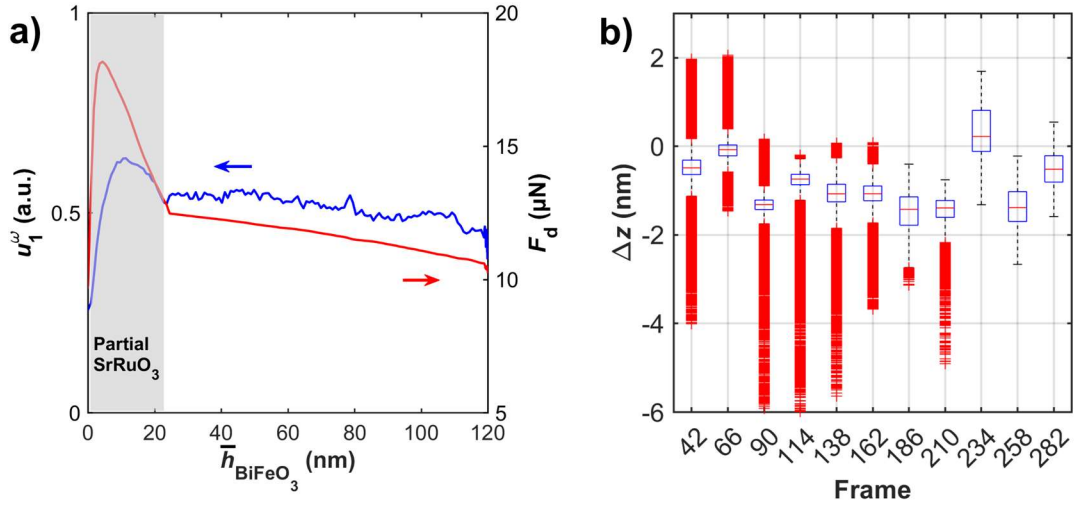

Fig. S3. PFM measurement fidelity during tomographic AFM. a) Local PFM piezoresponse serves as a proxy measurement of relative crystal quality; constant piezoresponse measured at a tip-sample contact resonance frequency implies no relative changes to the crystal structure within the electromechanical excitation volume of the PFM measurement(2). Shown here is the mean in-plane piezoresponse per frame, u_1^{ω} (solid blue line) as a function of mean $BiFeO_3$ film thickness ($\bar{h}_{BiFeO_3}$) measured in situ during tomographic AFM, which increases by ~26% over the course of the experiment. In contrast, a degradation of crystal quality generally presents as a strong reduction in piezoresponse. The magnitude of piezoresponse is known to be a function of cantilever downforce(3), here mean cantilever downforce per frame, F_d (solid red line) is shown to increase commensurately by ~17% during the tomographic AFM experiment. A large deviation in the piezoresponse is observed at a mean $BiFeO_3$ film thickness of 23 nm, which indicates when the underlying $SrRuO_3$ film has been partially revealed within the imaging field. Exposure of the $SrRuO_3$ conducting oxide alters the electrostatic boundary conditions present during PFM imaging, which presents a large anomaly in the apparent cantilever downforce due to the use of a metallic-like electrically conductive AFM probe. Although the cantilever downforce increases substantially when the $SrRuO_3$ is revealed, accurate determination of the film thickness can still be made using the z positioning sensor of the AFM. Likewise, the in-plane piezoresponse signal shown in this figure is a frame mean; localized regions that are less susceptible to the cross-talk effects of cantilever downforce can be identified and analyzed independently for the thickness-dependent analysis of functional properties. b) Statistical analysis of $BiFeO_3$ removal rate during tomographic AFM. a) Box plots showing median (red line), $25^{th}/75^{th}$ (blue box) and $5^{th}/95^{th}$ (black dashes) percentiles, and statistical outliers (red crosses) of the frame-to-frame material removal rate of $BiFeO_3$ during tomographic AFM. Δz represents the change in z height (film thickness) for a given imaging pixel between successive imaging frames. Panel b) represents a statistical treatment of the differential of the data shown in main paper Fig. 1c. A large number of statistical outliers observed below frame ~150, due to the tight statistical distribution of the as-grown film thickness during the early stages of tomographic AFM. Positive values of Δz, primarily observed at Frame 66 and below, are the result of imperfect spatial drift correction and topographic plane fitting of the data prior to tomographic analysis.

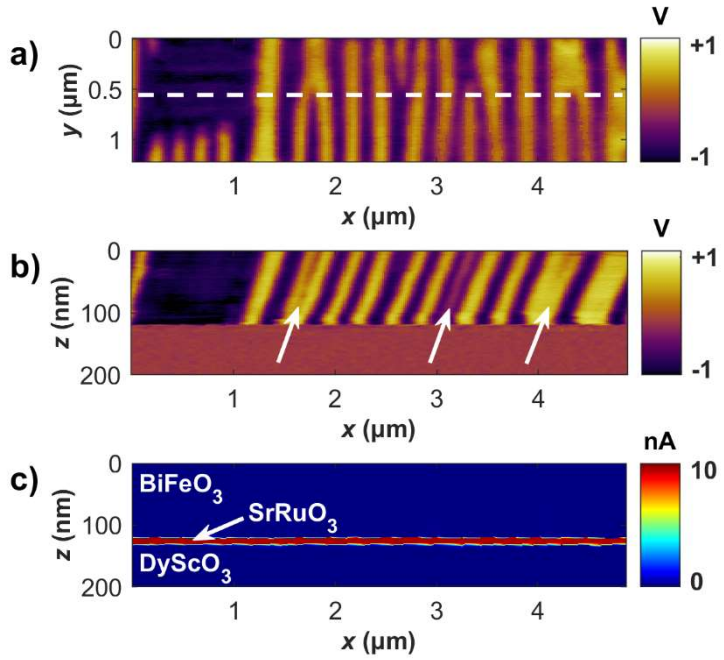

Fig. S4. Cross-sectional views of a $BiFeO_3$ thin film heterostructure acquired using tomographic AFM. a) Plan view (*x*-*y*) image of piezoresponse on $BiFeO_3$ at thickness h = 120 nm, showing stripe-type domain contrast of $[\bar{1}\bar{1}\bar{1}]$ and $[\bar{1}\bar{1}\bar{1}]$-oriented ferroelectric domains. b) *x*-*z* cross sectional image of piezoresponse on the $BiFeO_3$ heterostructure tomogram taken at y = 0.55 μm (white dashed line) from panel a). The z axis has been expanded by ~15x for viewing of cross-sectional domain geometry. White arrows indicate the locations of domain "bifurcations", as seen in panel a), revealing geometry that is nearly colinear to the $[101]_{pc}$ direction. c) Complementary *x*-*z* cross sectional image of probe current from the BiFeO*3* heterostructure tomogram, also taken at y = 0.55 μm in panel a). High probe currents (>10 nA, upper detection limit) on the conductive $SrRuO_3$ film relative to $BiFeO_3$ and the $DyScO_3$ substrate provide an unambiguous determination of the *z*-position at the $BiFeO_3/SrRuO_3$ and $SrRuO_3/DyScO_3$ interfaces, improving the spatial accuracy of the $BiFeO_3$ heterostructure tomograms.

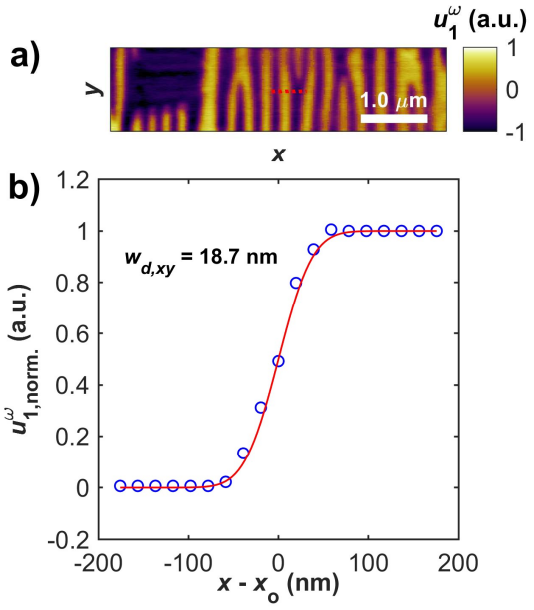

Fig. S5. Calculation of three-dimensional PFM property resolution on $BiFeO_3$ during tomographic AFM. Utilizing the method of Kalinin et al(4) for the calculation of image resolution during tomographic PFM imaging of $BiFeO_3$, a thorough analysis of the *x*-*y* and *z* spatial resolution within a tomographic AFM dataset has been performed. The imaging resolution of PFM can be determined by the change in PFM signal across a near-atomically sharp interface such as a ferroelectric domain wall or heteroepitaxial interface. The abrupt change in material properties, namely ferroelectric polarization, across such interfaces provides a platform for systematically assessing how the PFM contrast changes in response to such an interface, which can subsequently be used to extract the effective imaging resolution of PFM. In this context the imaged ferroelectric domain wall width is compared to the edge resolution in optical microscopy and can be used as a quantitative measure of the spatial resolution of PFM. The change in PFM response across a ferroelectric interface is commonly fit according to the function

$$R(x) = \frac{1}{2}\left(1 + \mathrm{erf}\left(\frac{wx}{\sqrt{2}}\right)\right) \quad (9)$$

where *R* is the piezoresponse, *x* is the spatial location relative to the interface (domain wall), and *w* is the domain wall width fitting parameter. The imaging resolution can then be written as $w_d = \sqrt{\pi/2}/(2w)$. In order to determine the imaging resolution of tomographic AFM, an in-plane ferroelectric domain wall, as well as the $BiFeO_3/SrRuO_3$ interface are used to determine the *x*-*y* and *z* components of the spatial resolution, respectively. a) Plan-view (*x*-*y*) image of in-plane piezoresponse (u_1^{ω}) of $BiFeO_3$ at the start of tomographic AFM. b) Cross-sectional (*x*-*z*) image of in-plane piezoresponse of $BiFeO_3$ taken along the dashed red line in panel a). b) Local statistical average of the in-plane piezoresponse (blue circles) across the domain wall marked with the dashed red line in panel a), fit with an error-function (solid red line) according to Eq. 9. Fitting of the data shown in panel c) results in an *x*-*y* spatial resolution of 18.7 nm, which is similar to values reported for PFM of ferroelectric oxides(4).

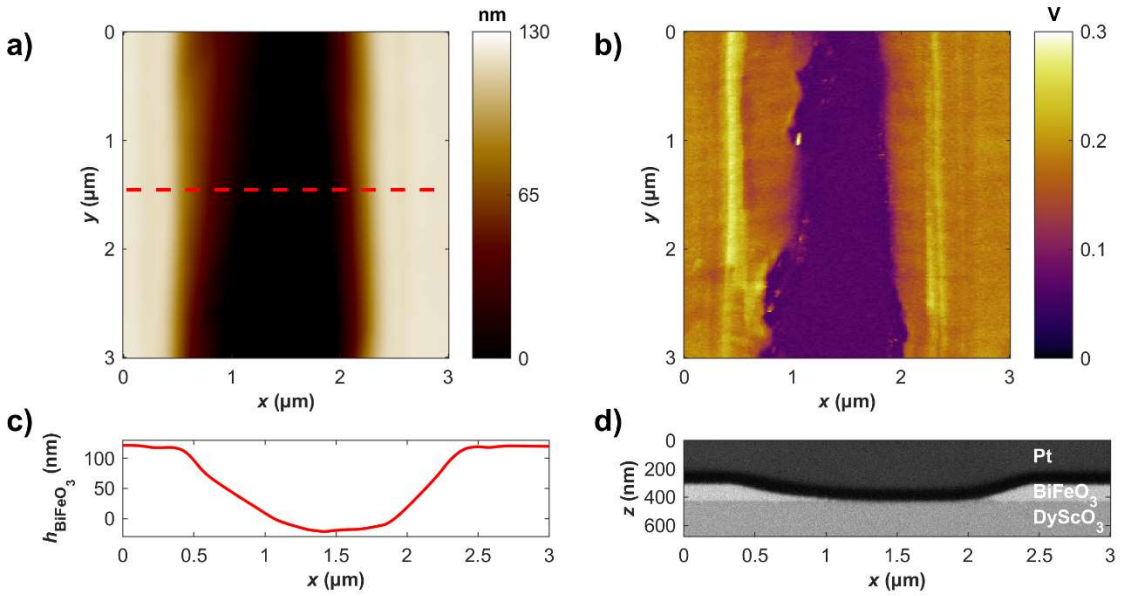

Fig. S6. *ex situ* measurement of a $BiFeO_3$ thin film heterostructure following tomographic AFM. a) AFM topography and b) local piezoresponse from a region of $BiFeO_3$ where tomographic AFM has been performed previously. Between x = ~1.0 μm and x = ~2.0 μm, the $BiFeO_3$ film has been completely removed as a result of the tomographic AFM process, with only $SrRuO_3$ and/or $DyScO_3$ remain. $SrRuO_3$ and $DyScO_3$ are non-piezoelectric materials and accordingly show only experimental noise-limited piezoresponse (~60 mV), substantially lower than that of $BiFeO_3$. c) Line scan of topography ($BiFeO_3$ thickness, h) from the dashed red line in panel a). d) Cross-sectional scanning transmission electron microscopy (STEM) image of the $BiFeO_3$ heterostructure following tomographic AFM, acquired on the $[010]_{pc}$ zone axis. The TEM cross section was extracted from the $BiFeO_3$ sample via focused ion beam milling at the dashed red line in panel a). Note complete removal of $BiFeO_3$ between x = ~1.0 μm and x = ~2.0 μm.

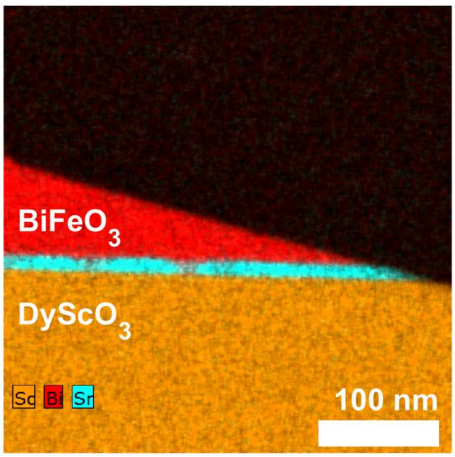

Fig. S7. Energy-dispersive x-ray spectroscopy (EDXS) image of a h = 120 nm $BiFeO_3$ thin film heterostructure following tomographic AFM. The change in film topography caused by the subtractive processing of tomographic AFM is clearly evident. Sharp film interfaces are observed with no apparent intermixing of chemical constituents between films, an indication of the minimal sub-surface damage induced by tomographic AFM.

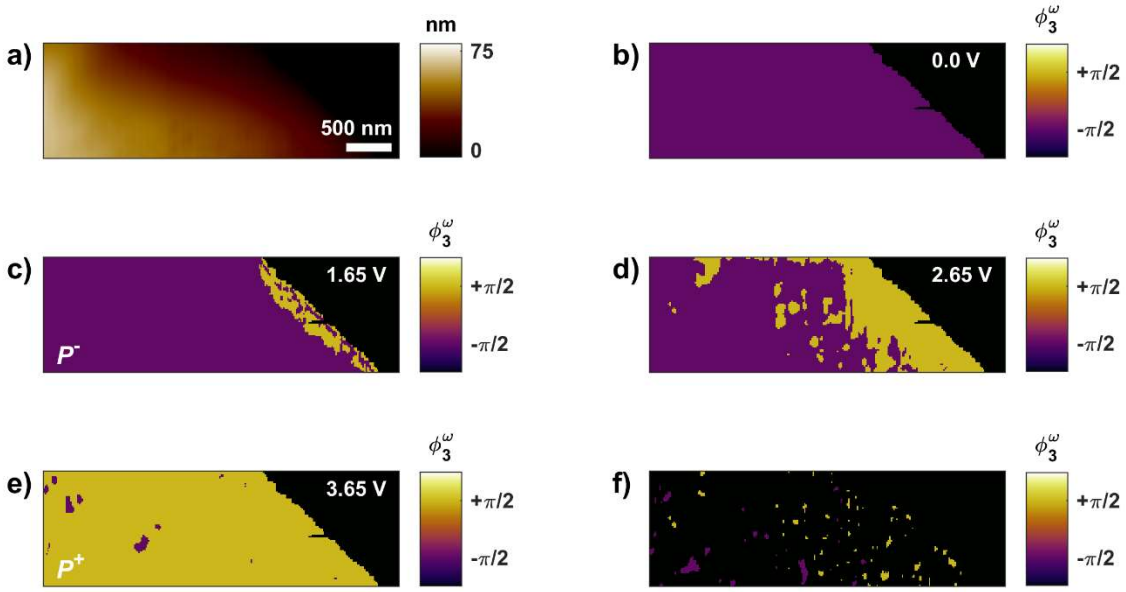

Fig. S8. Ferroelectric switching sequence of variable-thickness $BiFeO_3$. a) AFM topography (thickness, h) of $BiFeO_3$, b) out-of-plane PFM phase ($\boldsymbol{\phi_3^\omega}$) at the beginning of the switching sequence (V = 0.0 V) showing uniform P^- polarization. The black (null) region in panel b) corresponds to areas where the $BiFeO_3$ film has been completely removed by the tomographic AFM process; the [-π/2]-null interface indicates the zero-thickness limit of $BiFeO_3$. c) out-of-plane PFM phase at V = 1.65 V, showing switching of P^- (-π/2) to P^+ (+π/2) domains at $BiFeO_3$ thicknesses below ~20 nm. d) Out-of-plane PFM phase at V = 2.65 V and e) V = 3.65 V, showing evolution of switching as a function of applied voltage. f) Out-of-plane PFM phase from V = 2.65 V as in panel d), but with a numerical mask applied for identification of only P^+ domain nuclei. Individual domain nuclei were identified and isolated through manual procedure wherein each domain nucleus has been identified as a cluster of P^+ pixels that are present in a self-contained, distinct image region where no P^+ cluster existed in the previous frame(s). The film thickness (h) corresponding to V_c is calculated as the median thickness from the group of pixels that have switched from P^- to P^+ after the system has been held at an applied voltage (i.e. V_c), until the areal ratio of P^- to P^+ domains is invariant with respect to time. This procedure enables the highest-resolution results on thickness-scaling of E_c, and most closely embodies the nucleation-based theory proposed by Kay and Dunn(5).

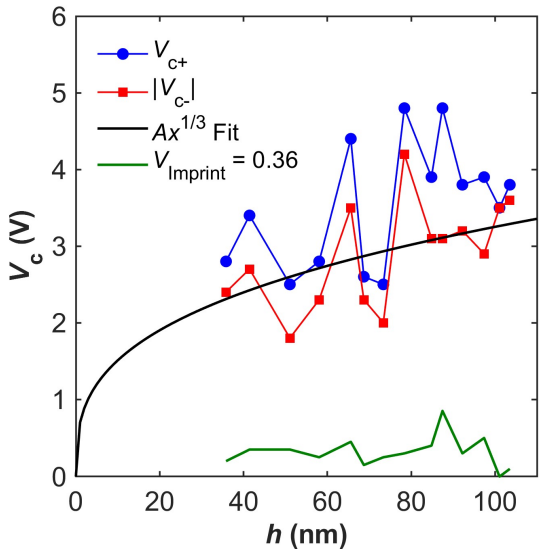

Fig. S9. a) Spectroscopic hysteresis of ferroelectric switching in variable-thickness $BiFeO_3$. Conventional quasi-static piezoresponse hysteresis loops, sweeping voltage from -5.0 V DC to +10.0 V DC at 0.1 Hz, were acquired at fourteen distinct $BiFeO_3$ thicknesses to supplement the results acquired from spatially-resolved switching sequences (i.e. main paper Figure 4). Positive coercive voltage (V_{c+}, blue circles) and the absolute value of negative coercive voltage ($|V_{c-}|$, red squares) are plotted versus $BiFeO_3$ film thickness (h), calculated as the zero-crossings of the out-of-plane piezoresponse phase ($\boldsymbol{\phi_3^{\omega}}$) averaged over ten switching cycles. A small ferroelectric hysteresis imprint (V_c asymmetry) is determined and plotted for each $BiFeO_3$ thickness (solid green line). The mean imprint voltage across the thickness range measured is 0.36 V; this imprint is compensated for in all spatially-resolved switching sequences. The imprint-compensated V_{c+} versus $BiFeO_3$ thickness has been fit to the power law equation $Ax^{1/3}$ (solid black line) using nonlinear least-squares regression, according to the semi-empirical Kay-Dunn scaling law(5). These results from discrete hysteresis loops generally follow power-law behavior, albeit with substantially higher experimental data scatter compared to the V_c versus h data shown in main paper Fig. 5.

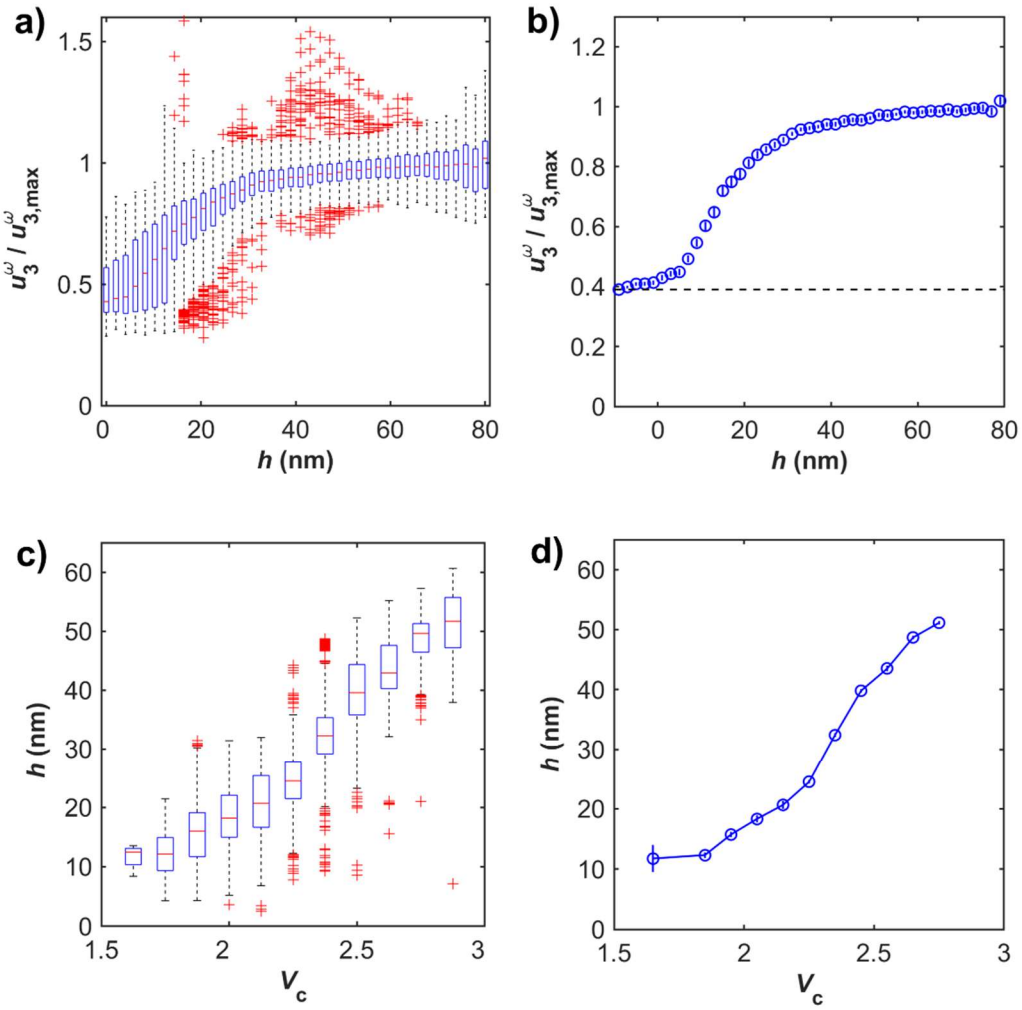

Fig. S10. Statistical analysis of depth dependent piezoresponse (as a measurement of spontaneous polarization, a-b) and coercive voltages (c-d). For both datasets, traditional 25th/75th percentile box plots, with the statistical median as well as distinct outliers also identified (red crosses), are displayed in (a,c). The median response is reproduced in (b,d), with 95% vertical confidence bars. The 95% confidence bars resulting from tomographic AFM are sufficiently small that they are nearly always encompassed by the data symbols shown.

References

1. Rault JE, et al. (2012) Thickness-dependent polarization of strained BiFeO3 films with constant tetragonality. *Phys Rev Lett* 109(26):267601.
2. Maksymovych P, et al. (2012) Ultrathin limit and dead-layer effects in local polarization switching of BiFeO3. *Phys Rev B - Condens Matter Mater Phys* 85(1):014119.
3. Kalinin S V., Bonnell DA (2002) Imaging mechanism of piezoresponse force microscopy of ferroelectric surfaces. *Phys Rev B* 65(12):125408.
4. Pennycook SVK and SJ and BJR and JS and APB and HNL and AB and SJ (2006) Spatial resolution, information limit, and contrast transfer in piezoresponse force microscopy. *Nanotechnology* 17(14):3400.
5. Kay HF, Dunn JW (1962) Thickness dependence of the nucleation field of triglycine sulphate. *Philos Mag* 7(84):2027–2034.